The Meteoritical Society

Meteoritics & Planetary Science 44, Nr 8, 1121–1132 (2009)
Abstract available online at http://meteoritics.org

Chemical identification of comet 81P/Wild 2 dust after interacting with molten silica aerogel

Frans J. M. RIETMEIJER

Department of Earth and Planetary Sciences, MSC 03-2040, University of New Mexico, Albuquerque, New Mexico 87131–0001, USA
*Corresponding author. E-mail: fransjmr@unm.edu

(Received 15 November 2008; revision accepted 15 June 2009)

Abstract–Flight aerogel in Stardust allocation C2092,2,80,47,6 contains percent level concentrations of Na, Mg, Al, S, Cl, K, Ca, Cr, Mn, Fe, and Ni that have a distinctive Fe- and CI-normalized distribution pattern, which is similar to this pattern for ppb level chemical impurities in pristine aerogel. The elements in this aerogel background were assimilated in non-vesicular and vesicular glass with the numerous nanometer Fe-Ni-S compound inclusions. After correction for the background values, the chemical data show that this piece of comet Wild 2 dust was probably an aggregate of small (<500 nm) amorphous ferromagnesiosilica grains with many tiny Fe,Ni-sulfide inclusions plus small Ca-poor pyroxene grains. This distinctive Fe- and CI-normalized element distribution pattern is found in several Stardust allocations. It appears to be a common feature in glasses of quenched aerogel melts but its exact nature is yet to be established.

INTRODUCTION

Paraphrasing Zolensky et al. (2006) on the nature of comet 81P/Wild 2 (hereafter Wild 2) dust: loose agglomerates of apparently intact terminal particles (up to 8–10 μm) at the end of the deceleration track, smaller, micrometer-scale particles mostly scattered along a narrow stylus, and numerous nanometer-scale particles that interacted with melted aerogel that are mostly found in the bulbous upper part of the deceleration track. The survival of hundreds of micrometer-scale mineral and polyphase mineral grains shows that the density-graded (0.01 to 0.05 g/cc) aerogel capture cells functioned as intended. It is not yet clear that these grains completely escaped some level of thermal or pressure-induced modifications. The majority of the nanometer-scale dust was petrologically modified when interacting with quantities of hypervelocity impact-generated silica (aerogel) melt (Leroux et al. 2008). We do not know the nature of this dust but we can make educated guesses of what it might have been by turning to chondritic aggregate interplanetary dust particles (IDPs) and the compositions of their individual constituents.

The most primitive extraterrestrial materials can be treated as a simple binary mixture of two chemical reservoirs: (1) a ferromagnesiosilica reservoir of mostly amorphous "silicate" materials and silicates (Rietmeijer 1996a, 1999, 2002) and (2) a Fe-Ni-S reservoir of Fe,Ni-sulfide and Fe,Ni-metal grains (Rietmeijer 2002, 2004). This binary mixture repeats itself during hierarchical, fractal dust accretion in the <500 nm-sized Principal Components (PCs) in the matrix of aggregate IDPs, in 10–15 μm chondritic aggregate IDPs, in cluster IDPs, and probably at larger scales also in comets (Rietmeijer 1998; Rietmeijer and Nuth 2004). Comet Wild 2 minerals (Brownlee et al. 2006; Matrajt et al. 2008; Zolensky et al. 2006, 2008) show a similar binary buildup, and I assume that it is dust that interacted with aerogel melt also had this binary nature.

The allocation described here came from a large (>10 μm), irregular (popcorn-like) clump of Si-rich glass with many macroscopic voids (cf. Rietmeijer et al. 2008; Nakamura et al. 2008). Its morphology gives the impression of an agglomerated mass of quenched glass blobs. Internally it is a silica-rich glass with numerous nanometer Fe,Ni metal and Fe-Ni-S compound inclusions very similar to previously studied Stardust glasses (Leroux et al. 2008; Nakamura et al. 2008; Rietmeijer et al. 2008; Tomeoka et al. 2008; Zolensky et al. 2008). The Si-rich matrix consists mostly of highly vesicular shards but non-vesicular "clean" glass shards are present. The latter is free of opaque inclusions although inclusions much smaller than ~10 nm might be present well below the surface of the typically 70 nm thick sections. Through-focus TEM imaging often reveals "shadows" of such scattered tiny inclusions.

Tomeoka et al. (2008) reported textural zoning in allocation C2027-2-69-1-4 that has (1) a core of Wild 2 olivine and pyroxene minerals, (2) a (partial) rim of Si-O-Al-rich

vesicular glass shards with variable amounts of Mg and Fe and with numerous electron-opaque Fe-Ni-S inclusions, and (3) an outer highly porous zone that is (flown) silica aerogel. Similar sharp glass-aerogel contacts are reported by Stephan et al. (2008) and Leroux et al. (2008), who also described transitions from pristine to densified (flown) aerogel and compressed aerogel. The contacts between these transitional forms are generally also sharp. Accepting this observed zoning as a model for the Si-rich glass clumps extracted from Stardust tracks, the two-dimensional sections cut from such clumps can also have non-vesicular glass as apparent inclusions but it mostly a rim on vesicular Si-rich glass. This massive, i.e., non-vesicular, clean glass rim can have an outer zone of recognizable porous aerogel in sharp contact.

The original aerogel is 99.5% SiO_2 plus ~0.5% residual hydrocarbons from the critical point extraction process and a wide range of element contaminants at ppb levels (Tsou et al. 2003). Also, particulate contaminants, e.g., sub-micrometer anhedral to euhedral calcite grains that is found principally in the loose chips of aerogel recovered from inside of the canister (Zolensky et al. 2006; Flynn et al. 2006; Supplemental data of both references). Contaminants can usually be easily recognized as such by their occurrence external to Wild 2 grains, i.e., they are situated in the enclosing shells of compressed to melted aerogel (Zolensky et al. 2006, supplemental data). Melting density-graded aerogel causes elements concentration and homogenization of particulate contaminants in silica melt. Several studies tried to establish contaminant backgrounds in the post-flight aerogel matrix using TOFF-SIMS and Synchrotron X-ray microbe analyses (Flynn et al. 2006; Ishii et al. 2008a; Lanzirotti et al. 2008; Stephan et al. 2008). So far, no chemically homogenous background was reported. Flynn et al. (2006; supplemental data) reported traces (ppm) of Ca, Fe, Ni, Cu, and Zn in track-free flight aerogel of cell C2054,8 that are frequently localized in "hot-spots," in particular Ca hot spots, throughout the aerogel.

The flight aerogel in the Stardust allocation described contains measurable amounts of various elements detectable by energy dispersive spectroscopy (EDS) analyses that could be indigenous aerogel contaminants or Wild 2 "chemistry" that penetrated the flight aerogel. I report the presence of an aerogel background of Na, Mg, Al, S, Cl, K, Ca, Cr, Mn, Fe, and Ni. The pattern of the normalized element abundances strongly suggest that they are enhanced indigenous (pre-flight) aerogel contaminants. Removal of all element abundances corresponding to the aerogel background, and subtracting the appropriate background values from the remaining data, brings out chemical trends that can be traced to comet materials.

SAMPLE AND EXPERIMENTAL PROCEDURES

The Si-rich glass clump was extracted from the wall of track #80 in keystone C2092,3,80,0,0 (Fig. 1). This particle, C2092,2,80,47,0 was located ~400 μm below the entrance hole (Fig. 2). Allocation C2092,2,80,47,6, which was embedded in Embed812 epoxy in the NASA Johnson Space Center Stardust Curatorial Facility, contains five serial, ultrathin (~70 nm) transmission electron microscope (TEM) sections (#22–#26) on a 10 nm thick amorphous carbon film that is supported by a standard Cu TEM grid. The sections present a 3-D slice through a fragment of this particle. Each TEM section was exhaustively analyzed.

The analyses were performed using a JEOL 2010 high-resolution transmission electron microscope (HRTEM) that operated at a 200 keV accelerating voltage and was equipped with an ultrathin-window energy-dispersive X-ray detector for quantitative chemical analyses, including oxygen, using the standard Cliff-Lorimer thin film procedure at UNM (cf. Zolensky et al. 2006, supplemental data). The focused analytical probe size (5, 10 or 15 nm) was selected to be smaller than the object of interest wherever possible but maintaining an optimum combination of electron beam probe size and EDS acquisition time (fixed) to ensure statistically relevant signal-to-noise ratios. The data reduction program indicates when an element is present near the two-sigma level for most of the element abundances in flight aerogel and massive glass that have very high aerogel and glass to comet dust ratios. Using the most appropriate analytical spot size, I randomly probe many spots in the vesicular and massive glasses and in flight aerogel. A spot analysis of an electron-opaque inclusion >35 nm tends to be "clean," i.e., it has no or very little admixed glass chemistry. With decreasing inclusion size the amount of glass chemistry increases along the mixing lines. In this approach the compositions of the smallest inclusions cannot be obtained. Their identification requires HRTEM element mapping, lattice imaging, and convergent beam electron diffraction. Silica aerogel was contaminated with comet Wild 2 (Rietmeijer 2007), which means that glass compositions define linear mixing lines between SiO_2 and captured comet dust compositions. When trying to reconstruct the chemical properties of comet's dust I will use a binary presentation of Si (el%) versus an element of choice contributed by the comet. In this manner the amounts of a Wild 2 element will decrease to very low abundances to their aerogel background level at high Si (el%) contents.

OBSERVATIONS

In each of TEM section of allocation C2092,2,80,47,6 three materials are analyzed, viz. (1) vesicular Si-rich glass with numerous electron-opaque inclusions <100 nm, (2) inclusion-free massive Si-rich glass that mostly surrounds vesicular glass, and (3) aerogel. Probing the sections with a focused beam reveals variable element abundances, including zero (undetectable) amounts, at a scale of >25 nm but less than ~100 nm. The upper value is a best estimate. Similar scales of chemical heterogeneity are caused by the

Fig. 1. Optical image of track #80 in the C2092,3,80,0,0 keystone. The maximum width of this bulbous, Type B, track is ~1700 μm. The entrance hole (at the bottom of this image) is ~410 μm; its length/depth ratio is ~4,694 μm. Grain diameters range from about a few microns to ~30 μm. There are three terminal particles on the order of 15, 8, and 7 μm in size at the end of three styli that measure on the order of ~4800 and 4475 μm in length (source: NASA Johnson Space Center Stardust curatorial website).

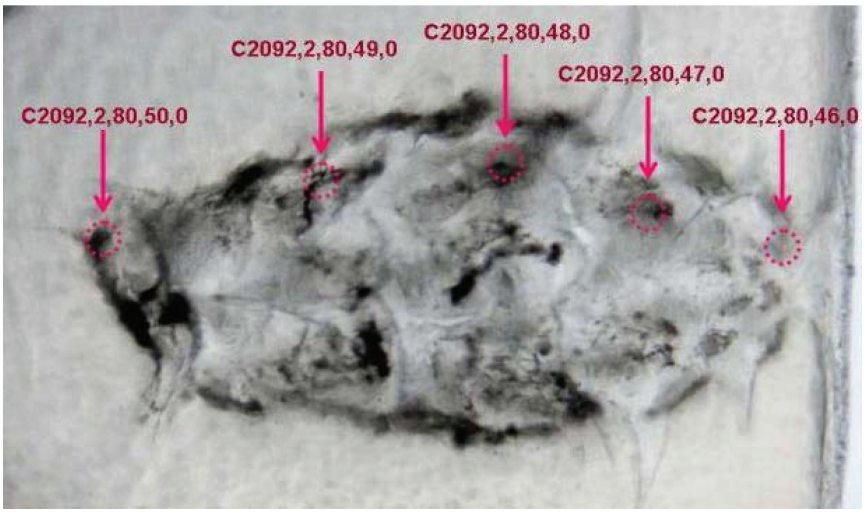

Fig. 2. Optical image of track #80 in the C2092,3,80,0,0 keystone showing the location of grain C2092,2,80,47 from which allocation #6 is the subject of the present study. The entrance hole is located at the right hand side of the image. The image is reproduced by courtesy of the NASA/JSC; Stardust curatorial website.

random distributions of Fe,Ni-metal and Fe-Ni-S inclusions and their variable sizes from ~1 nm up to ~100 nm. There are no obvious differences among the five TEM sections. The data shown are the average abundances (elemental/atomic).

The flight aerogel uniformly contained measurable amounts of various elements. The calculated average of these elements in this aerogel (Table 1) are compared to the values for the same elements present at ppb levels in pristine (pre-flight) aerogel (Tsou et al. 2003) (Fig. 3). For comparison, the Fe-normalized abundances are also CI-normalized (Anders and Grevesse 1989) which reveals the remarkable similarity of the distinctive pristine and flight aerogel distribution patterns. The sulfur abundances suggest that the physical process or processes causing these enhancements in flight aerogel did not act in the same manner for this element. Chlorine in flight aerogel of this allocation is enigmatic, as it was not listed among the elements present in pristine aerogel although chlorine is associated with aerogel in some Stardust samples (Ishii et al. 2008a).

The overall patterns of the aerogel background abundances in allocation C2092,2,80,47,6, and in the aerogel backgrounds of allocation C2115,34,21,0; slice 6 (Stephan et al. 2008) and track C2115,19 (Lanzirotti et al. 2008), are similar (Fig. 4). There are differences. For example, a factor of 10 difference in the Cr/Fe and Mn/Fe

Table 1. Element flight aerogel background abundances (element and atomic percentages) in Stardust allocation C2092,2,80,47,6.

	Element %	Atomic %
Na	0.4	0.38
Mg	0.4	0.6
Al	0.3	0.2
S	0.4	0.4
Cl	1.2	0.7
K	0.12	0.06
Ca	0.1	0.05
Cr	0.24	0.1
Mn	0.16	0.06
Fe	2.4	2.4
Ni	0.8	0.4

Note: the Al data are based on four data points.

abundances between allocations C2092,2,80,47,6 (reported here) and C2115,34,21,0; slice 6. Even more dramatic is the factor of 100 difference in the Ca/Fe abundance in track C2115,19. In this normalization procedure the iron content becomes a variable parameter, which suggests that the scale at which comparisons are made, i.e., an entire track, or aerogel in bulk sample, or aerogel in ultrathin TEM sections, becomes important. Comparisons among aerogel samples appear to be reasonable.

Flight aerogel is frequently in sharp contact with the massive glass. This clean glass is entirely devoid of electron-opaque inclusions, with the caveat of grain size versus section thickness. It can have a very fine powder "dusting" of ~1-nanometer-sized inclusions that is uncommon in vesicular glass. The distribution patterns for the Fe- and CI normalized element abundances of the aerogel background and this clean massive glass are very similar (Fig. 5). The difference above the flight aerogel abundance of the Mg/Fe abundance in the massive glass is real. It suggests that some fraction of Mg in the massive glass is derived from an external source that was the comet itself. The difference in the Al/Fe abundances might be real but the data set is too small to allow a definitive statement.

The data (Fig. 5) support that the massive (non-vesicular) glass is an (almost) isochemically quenched glass from hypervelocity impact-generated molten aerogel that with regard to Mg, and probably Fe, is compositionally intermediate between the flight aerogel and vesicular glass chemistries. The sharp contacts between massive (non-vesicular) and vesicular glasses indicate that some fraction of Mg and Fe could diffuse into the massive glass zone rather than being mixed as ferromagnesiosilica melts. It suggests that aerogel melting and quenching proceeded faster than these element diffusion times in silica at the high temperatures of capture.

In a conservative approach, and assuming all Si-rich glass is derived from melted aerogel, I subtract the background value (see Table 1) from each individual analysis of vesicular glass. In this manner I obtain a chemical signature of the comet dust before it reacted with the Si-rich melt that was contaminated with the flight-aerogel background abundances. I ignore the likely silica contributions from indigenous amorphous silica-bearing materials and silicates in the comet because I do not have any way to ascertain this contribution to the melt. The results show that (1) Mg, S, Ca, Cr, Mn, Fe, and Ni are present in variable, relative amounts throughout the vesicular and massive glass, (2) Na or Cl occur in only a few spots these glasses, (3) above-background Al is found in a single spot in vesicular glass, and (4) there is no potassium above its background value. After background subtraction Mn and Cr associated with metal and Fe-Ni-S inclusions may form hot spots at spatial scales that correlate with the distributions of these inclusions.

BULK COMPOSITION

When potential contaminant abundances are associated with a particle track, their origin, i.e., contamination or comet material, cannot be unambiguously identified and when contaminant elements form "hot spots" it becomes very difficult to decide the proper procedure to apply a whole-track contaminant background (Flynn et al. 2006). It may be less of a problem to apply a contaminant background correction to comet grain abundances when comet Wild 2 dust was assimilated in quenched silica glass. At this scale, I think that the conservative approach of this study is justified. That being said, the aerogel background-corrected elements then show the average Fe- and CI-normalized abundances of the Wild 2 dust in vesicular glass of allocation C2092,2,80,47,6. This piece of the comet has a chondritic composition for Cr, Mn, Fe and Ni, but <CI abundances for Na, Mg, Ca, and sulfur (Fig. 6). The Fe- and CI-normalized and background-corrected abundances for vesicular glass in allocation C2115,34,21,0; slice 6 (Stephan et al. 2008), and the Ca, Cr, Mn, and Ni abundances in 24 individual Stardust deceleration tracks (Flynn et al. 2006), resemble the abundances for the vesicular glass of allocation C2092,2,80,47,6 (Fig. 7). There are differences for Ca in the whole track abundances, an indication that the scale at which comparisons are made should be considered. The differences between the Fe-normalized Mg and Na abundances in both aerogel samples may be individual track signatures or due to differences in the applied analytical procedures.

GLASS COMPOSITIONS

The compositions of Si-rich glasses extracted from the deceleration tracks are linear mixtures of CI-like comet dust and melted silica aerogel (Leroux et al. 2008). I assume that (1) chondritic pieces of comet Wild 2 dust interacting with silica melt and aggregate IDPs are both binary mixtures of

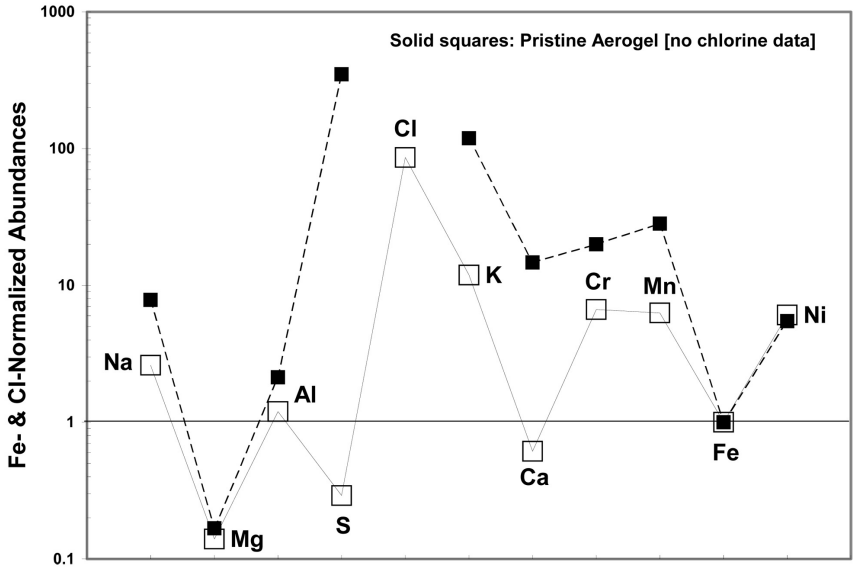

Fig. 3. The Fe- and CI-normalized element abundances at percent levels measured in porous, flight aerogel of allocation C2092,2,80,47,6 (open squares) are compared to the same elemental abundances but at ppb levels in pristine aerogel (Tsou et al. 2003). The pattern of the elemental aerogel background (solid lines) is quite characteristic.

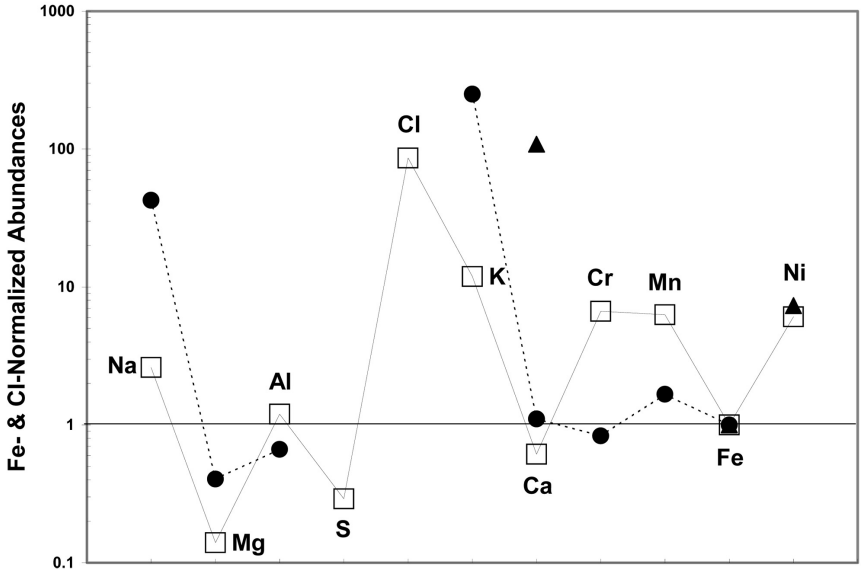

Fig. 4. Comparison of the Fe- and CI-normalized elemental abundances of the aerogel background in allocation C2092,2,80,47,6 (open squares) compared to flight aerogel backgrounds in Stardust allocations C2115,34,21,0; slice 6 (dots; Stephan et al. 2008) and flight aerogel from track C2115,19 (solid triangles; Lanzirotti et al. 2008).

two chemical reservoirs, and (2) all iron is present Fe,Ni-metal, Fe,Ni-sulfides and Fe-S compounds (≤70 nm) with a deep metastable eutectic compositions either close to FeS or at Fe:S = 80:20 (Rietmeijer 2008; Rietmeijer et al. 2008). I then use this graphical presentation (Fig. 8) to explore trends in background-corrected compositions. The compositions obtained by spot analyses for most of the Ni-free and low-Ni electron opaque inclusions in the silica glass will be along the dotted mixing lines (Fig. 8) towards the aerogel background values between ~44 and ~46 Si (el%). The compositions of Fe-Ni-S compound grains, and Fe,Ni-sulfides that are ~70 nm and larger will be Si-free. The compositions on these mixing lines are a crude indicator of inclusion size. The "silicate line" (Fig. 8) identifies the Si (el%) range for olivine, Ca-free and low-Ca pyroxenes and Ca-rich clinopyroxenes in IDPs represented by chondritic aggregate IDP L2011A9. The silicates in this IDP are common to many other aggregate IDPs (Rietmeijer 1998, 1999; Zolensky and Barrett 1994). These silicates with ~12 to

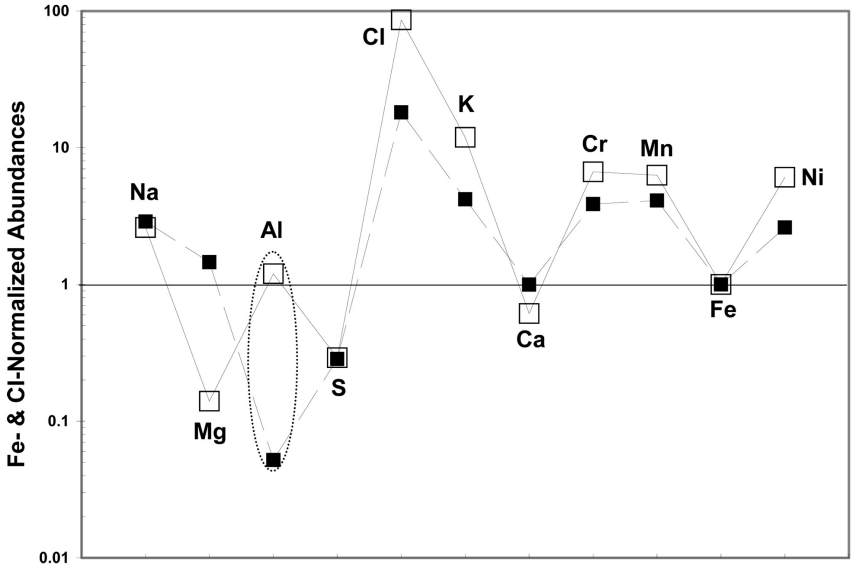

Fig. 5. Comparison of the Fe- and CI-normalized element distribution patterns of the aerogel background in allocation C2092,2,80,47,6 (open squares) and the same elements in massive, i.e., non-vesicular glass (solid squares). The aluminum abundances bracketed by the dashed oval are based on very small number statistics. The size of the oval is entirely unconstrained and needs more data.

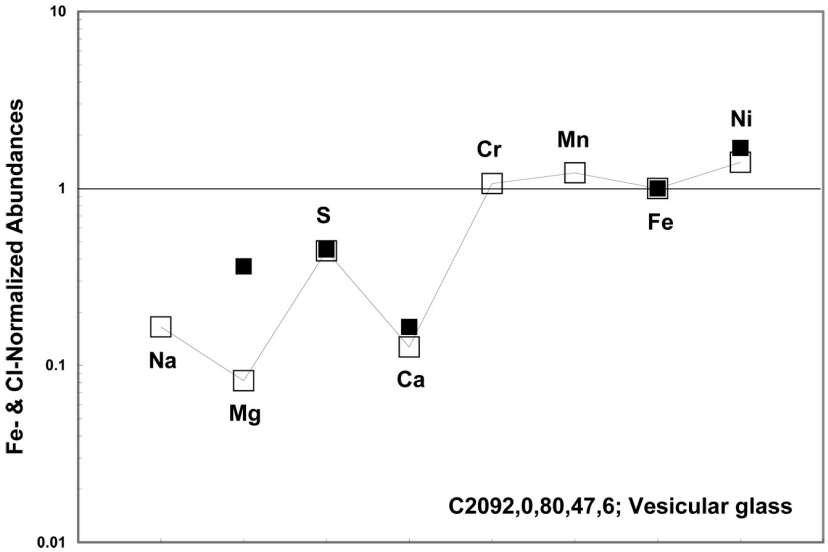

Fig. 6. The Fe- and CI-normalized, and aerogel-background-corrected, bulk elemental abundances of the Wild 2 dust that contaminated the hypervelocity impact generated Si-rich vesicular glass in allocation C2092,2,80,47,6.

~35 Si (el%) contribute Mg and silica to the aerogel melt wherein they are completely assimilated. There is no Mg (other than background) between zero and ~12 el% Si (Fig. 8).

The anti-correlated Mg abundances in massive, almost pure magnesiosilica, glass lie on an extension of the silicate line (Fig. 8) but cannot be from silicates. The maximum MgO content of 19 wt% matches the deep metastable eutectic smectite-dehydroxylate composition of condensates obtained in laboratory vapor phase condensation experiments (Rietmeijer et al. 2002). In the condensing Mg-SiO-H_2-O_2 vapors pure MgO and pure silica vapors mixed to produce magnesiosilica condensates. Cautiously at this time, these massive glass compositions may be the first evidence that vapor was generated during hypervelocity impact capture.

I assumed that the vesicular magnesiosilica glass is Fe-free, which is indeed the case (Fig. 9; diamonds); only few spots in vesicular and non-vesicular glasses have a ferromagnesiosilica composition (Fig. 9). This assumption is corroborated by the high incidence of cooccurring Fe and S compositions (Fig. 10, dots). The amount of iron in glass that is not associated with the inclusions, is typically <15 (el%) and Si >35 el% (Fig. 10).

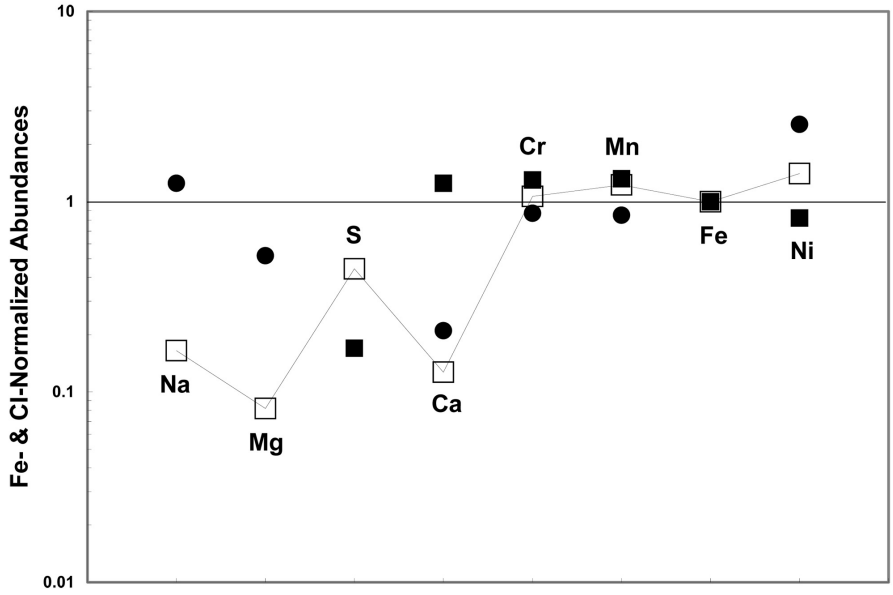

Fig. 7. Comparisons of Fe- and CI-normalized, and aerogel-background-corrected, bulk compositions for C2092,2,80,47,6 (open squares), allocation C2115,34,21,0; slice 6 (dots; Stephan et al. 2008) and 24 whole track abundances (solid squares; Flynn et al. 2006).

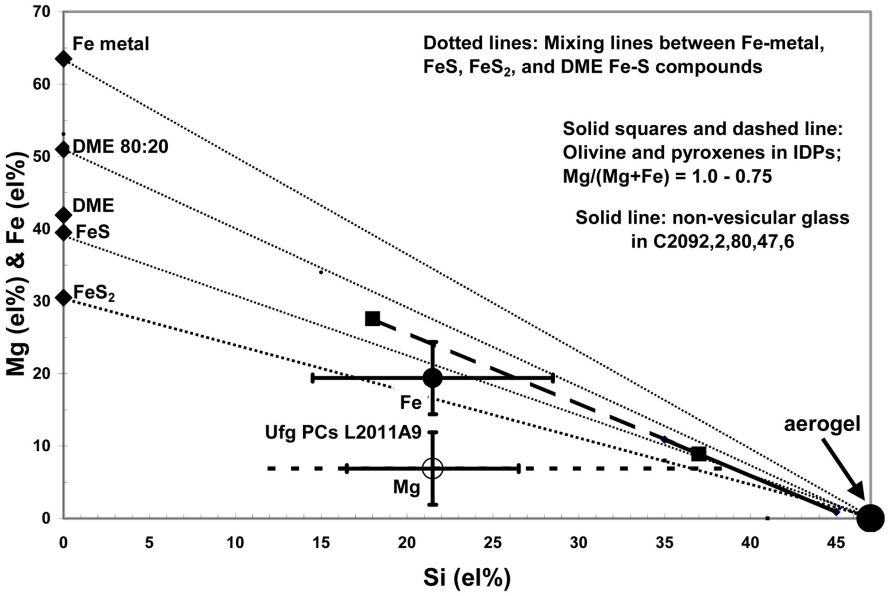

Fig. 8. This Mg and Fe (el%) versus Si (el%) diagram is used as a simple tool to showing the chemical mixing of Fe,Ni-sulfides, Fe-Ni-S compounds, or both (Fe versus Si) (dotted lines), and amorphous "silicate" materials and silicates, typically olivine and pyroxene (Mg versus Si), in comet Wild 2 samples. Iron is mostly present in Fe-metal, "FeS" (cf. Zolensky et al. 2006), FeS_2 and two Fe-S compounds with a deep metastable eutectic in the Fe-S phase diagram (Rietmeijer 2008, Rietmeijer et al. 2008) (solid diamonds). The olivine and pyroxene compositions and average Fe (solid square) and Mg (open circle) compositions, both with 10% error bars, of ultrafine-grained principle components in chondritic aggregate IDPs are shown, using IDP L2011A9 as a representative particle (Rietmeijer 1994, and unpublished data). Including the range for Mg compositions in ufg PCs (dotted line), Si contents between ~15 and ~40 el% will be a mix of Wild 2 and aerogel silica. The solid extension of the "silicate" line delineates the Mg versus Si compositions in non-vesicular glass of allocation C2092,2,80,47,6 (see text). The big dot in the lower right-hand corner represents 100% pure aerogel.

Preliminary data suggest that silicates >500 nm survived in vesicular glass (Leroux et al. 2008) but there are no surviving silicates in this allocation. What then can we infer for the nature of likely precursor, i.e., Wild 2 minerals or phases? Chondritic aggregate IDPs contain ultrafine-grained (ufg) PCs that have an amorphous ferromagnesiosilica matrix with numerous nanometer-size electron-opaque inclusions (Rietmeijer 1994, 2002). Their origin is unknown. It has been

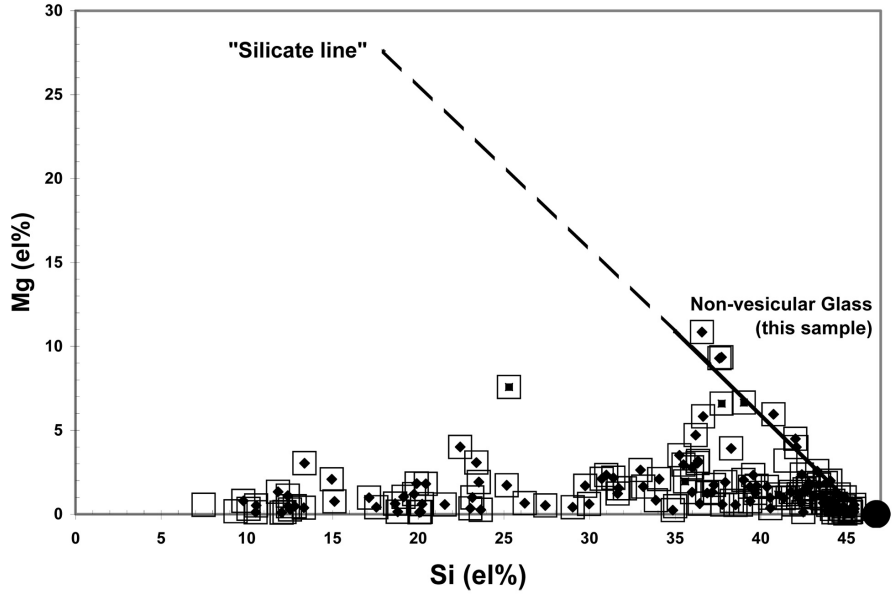

Fig. 9. Mg versus Si (el%) diagram showing the background-corrected vesicular glass compositions in allocation C2092,2,80,47,6 (open squares), incl. non-vesicular glass along solid extension of the IDP L2011A9 silicate line. A solid diamond marks pure-Mg glass compositions; an empty open square designates the presence Mg and Fe, and in some instances, also Ca. The big dot in the lower right-hand corner represents 100% pure aerogel.

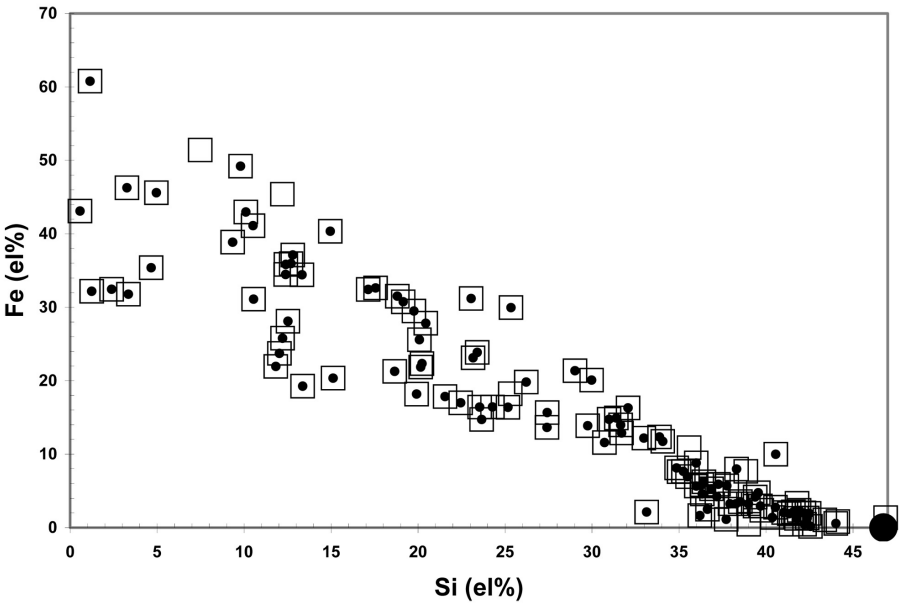

Fig. 10. Fe versus Si (el%) diagram showing all background-corrected, Fe-containing compositions obtained in allocation C2092,2,80,47,6 (open squares) and wherein sulfur is present (dots) that correspond to the electron opaque inclusions and S-free glass (empty open squares). Both high-Fe data points in the upper left are Fe,Ni-metal. The big dot in the lower right-hand corner represents 100% pure aerogel.

hypothesized that they could be chemically evolved, non-equilibrium vapor phase condensates (Rietmeijer 2002). Their petrological and chemical properties (Rietmeijer 1989, 1993) are similar to those of the GEMS (Bradley 1988, 1994; Joswiak et al. 1996) that were hypothesized (Bradley and Ishii 2008) to be pre-accretionally irradiated grains prior to accretion into comets. None of ufg PC properties support irradiation-induced modifications such as partial amorphization of (relic) grains or vesicular textures. When lacking such conclusive evidence, I prefer the descriptive designation of ufg PCs. Their average Mg and Fe (el%) contents have a slightly wider range of Si (el%) contents than silicates (Fig. 8). The low Mg content is a useful discriminator of ufg PCs and silicates. Two amorphous Ca-bearing ferromagnesiosilica glass compositions in this allocation have Mg and Fe (el%) values matching the ufg PC values. Its Ca/Si

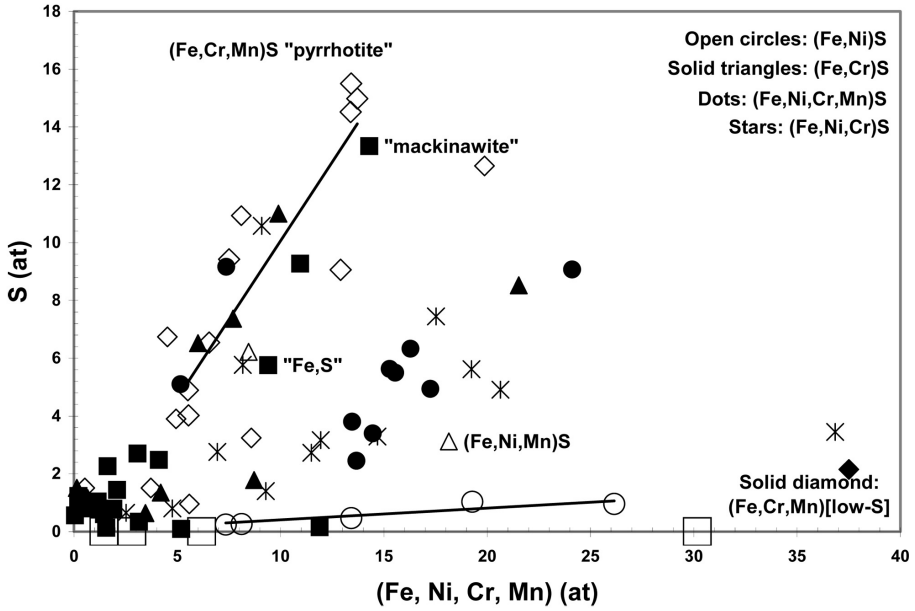

Fig. 11. (Fe,Ni,Cr,Mn) versus Si (atomic %) compositions of electron-opaque inclusions in vesicular glass in allocation C2092,2,80,47,6 showing the diversity of chemical heterogeneity. The data points <5 at% for (Fe,Ni,Cr,Mn) and sulfur are mostly the smallest inclusions.

ratio is also consistent with ufg PCs (Rietmeijer 2009). The Mg/(Mg+Fe) (*mg*) element ratios of vesicular ferromagnesiosilica glass are discontinuous, viz. (1) low-*mg* (0.15 to 0.35) ratios and (2) high-*mg* (0.85 to 0.93) ratios. So far, few olivine or pyroxene compositions among the surviving Wild 2 silicates and in aggregate IDPs match the low-*mg* group. The ufg PCs in aggregate IDPs show a similar discontinuity (Rietmeijer 1996b, 1998). About 25% of vesicular magnesiosilica glass contains small amounts of calcium. The mean Ca/Mg ratio, 0.12 ± 0.07 (range: 0.02–0.35), is consistent with the range for ufg PCs (Rietmeijer 2009). This ratio for glass ranging from ~10 to ~44 Si (el%) might point to a precursor in this Wild 2 dust that was probably low-Ca pyroxene. It is the only known silicate with this ratio in aggregate IDPs (Rietmeijer 1998). In summary, the Mg, Fe and Ca data suggest that the tiny piece of comet Wild 2 that left its imprint in the vesicular glass of allocation C2092,2,80,47,6 chemically resemble ufg PCs with perhaps small low-Ca pyroxene minerals.

FE-NI-S COMPOUND COMPOSITIONS

The Fe-Ni-S (at%) aerogel background in a ternary presentation forms a small cluster centered on Fe:Ni:S = 73: 15:12. The electron-opaque inclusion data, but uncorrected for the background values (cf. Table 1), show bewildering combinations of Fe, Ni,Cr-metal and (Fe,Ni,Cr,Mn)-S compositions (Fig. 11). Broadly, the (Fe,Ni,Cr,Mn)S compositions divide in Mn- and Ni-containing compounds (Fig 11; dots). In general, the Mn and Cr contents are so low that they don't show in the second decimal of the calculated chemical formulae for the background corrected data (Table 2). Using the composition of the largest inclusion in each group (Fig. 11), I reduced the data as pyrrhotite, $Fe_{1-x}S$ or mackinawite, $Fe\text{-}S_{1-x}$ (Table 2). The metal compositions include pure-Fe, Fe,Ni and Fe,Cr compositions. The compounds that are not stoichiometric pyrrhotite or mackinawite that coincides with one of the deep metastable eutectic Fe-S compositions (Rietmeijer 2008, Rietmeijer et al. 2008), are coincident with the second DME Fe-S compound or have a low-S eutectic composition (Fig. 11; solid line through open circles). The relative distributions of Fe, Ni, Cr and Mn (at) are completely independent of sulfur content.

DISCUSSION AND CONCLUSIONS

This allocation contains no recognizable surviving Wild 2 mineral grains in the silica melt. Flight aerogel in allocation C2092,2,80,47,6 percent levels of Na, Mg, Al, S, Cl, K, Ca, Cr, Mn, Fe, and Ni. Its distinctive pattern of these Fe- and CI normalized element distributions is identical to the distributions of the same elements in pre-flight aerogel and clean massive glass in contact with flight aerogel. The massive glass also shows Mg- and Fe-signatures caused by comet dust. This allocation, as most others of its kind already reported in the literature, is dominated by vesicular glass that is the result of a tiny piece of Wild 2 dust interacting with melted aerogel that already contained the background elements. The vesicular glass data corrected for the aerogel background values show that (1) Mg, Al, Ca, and a small fraction of Fe from the comet assimilated fairly homogeneously in the melt although hot spots (Ca, Al) exist and (2) S, Fe, and Ni formed immiscible sulfide melts that quenched as (sub) spherical Fe-Ni-S compound droplets that

Table 2. Aerogel background corrected Mn, and Cr (or both) bearing Fe-Ni-S compound compositions scattered throughout vesicular glass in Stardust allocation C2092,2,80,47,6. The mackinawite, pyrrhotite, and intermediate formulae are without presumption of a crystalline nature.

Metals	Intermediate FeS_{1-x} compounds	"Mackinawite" FeS_{1-x}	"Pyrrhotite" $Fe_{1-x}S$
Pure Fe			
$Fe_{0.9}Cr_{0.1}$	$FeS_{0.85}$	$FeS_{0.9}$	
$Fe_{0.9}Ni_{0.1}$	$FeS_{0.6}$		$Fe_{0.88}Ni_{0.02}S$
	$FeS_{0.4}$		
	$Fe_{0.96}Ni_{0.4}S_{0.05}$		
			$Fe_{0.89}Cr_{0.02}Mn_{0.01}S$
	$Fe_{0.94}Ni_{0.05}Cr_{0.01}S_{0.1}$		
	$Fe_{0.9}Ni_{0.05}Mn_{0.05}S_{0.2}$		
	$Fe_{0.97}Ni_{0.02}Cr_{0.01}S_{0.3}$		$Fe_{0.96}Ni_{0.01}Cr_{0.03}S$
	$Fe_{0.94}Ni_{0.05}Cr_{0.01}S_{0.4}$		

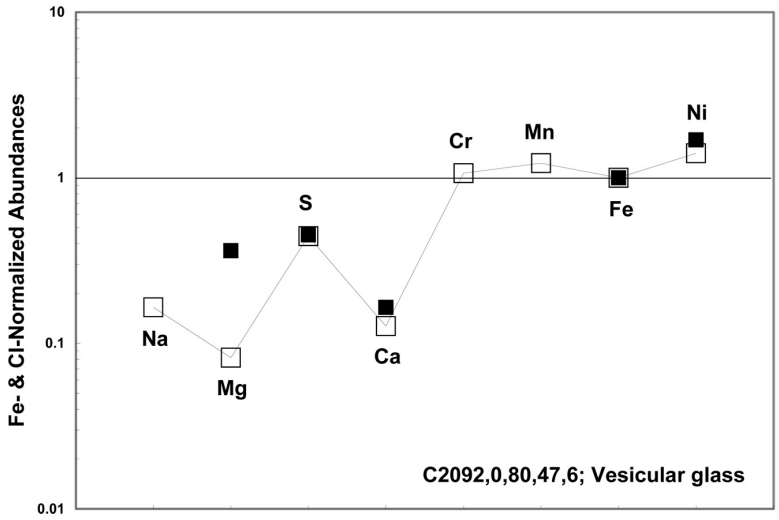

Fig. 12. The Fe- and CI-normalized elemental abundances in vesicular glass of allocation C2092,2,80,47,6 (open squares) compared to the same elements in ufg PC compositions in aggregate IDP L2001A9 (solid squares; Rietmeijer 2009). There is no measurable Na and Cr in ufg PCs.

may reflect a complex phase chemistry in Fe,Ni,Cr,Mn-sulfur alloy systems.

The background corrected bulk composition of the vesicular glass composition of this allocation is very similar to the Fe- and CI-normalized ufg PC compositions in IDP L2001A9 (Fig. 12). This piece of comet Wild 2 dust consisted of ufg PCs with perhaps embedded small low-Ca pyroxene minerals. The ultrafine-grained PCs are texturally and chemically similar to GEMS, but their origins could be different. Electron-opaque inclusions in the ufg PCs in three aggregate IDPs range from ~1 nm to 35 nm, with very few inclusions up to 90 nm (Rietmeijer 1994; L2011A9 was misidentified as U2011A9). Including the larger size, this range covers the entire range of Fe-Ni-S inclusion sizes in allocation C2092,2,80,47,6.

We do not yet fully understand the hypervelocity capture process in terms of textural and chemical dust modification. This work shows that the preserved chemical signatures mimic those of some of the constituents in aggregate IDPs. Chemical diffusion in the Si-rich melt was apparently very limited. There is textural evidence from the largest and typically zoned Fe-Ni-S compound grains (Leroux et al. 2008) to suggest they moved through the melt (Rietmeijer 2008). The chemical zoning of Fe-Ni-S compounds in Stardust glass has not yet been seen in aggregate IDPs. Ishii et al. (2008b) produced similar zoning in hypervelocity impact experiments that simulated the Stardust capture process and found zoned compounds that might be a unique Stardust feature. The glass particle (C2092,2,80,47) from which this allocation was prepared was probably an aggregate Wild 2 grains with an ufg PC composition. The sizes of electron-opaque inclusions in ufg PCs (Rietmeijer 2009) are similar to the Fe-Ni-S compound sizes in vesicular glass (Leroux et al. 2008). Perhaps the Fe-Ni-S compounds as found in the glass still have their original (pre-capture) sizes, which implies that the chemical zoning is an impact related

feature. It is also possible that the largest Fe-Ni-S droplets in this allocation grew in situ by agglomeration and fusion of small droplets during hypervelocity capture. This scenario would concentrate Mn and Cr in relatively rare large Fe-Ni-S droplets. This is consistent with the chaotic distribution of Fe,Ni,Cr,Mn-S compound compositions (Fig. 11) whereby the smallest grains contain Mn and Cr in concentrations barely above the aerogel background values.

This work raises other issues. Namely, does each track have its own aerogel background or does each extracted grain have its own unique background. Or, is there a common post-flight Stardust aerogel background? Does it even matter? Assuming a common aerogel background, what would be the impact on the compositions of minerals that survived intact? I would think that it would not be severe as for single crystals wherefore a stoichiometric composition offers a check. A background either common or "local" will have to be considered for amorphous materials and especially vesicular and massive glasses as described here. I do not know if the element concentration factors in the flight aerogel described here is the norm or high. Obviously more data are needed but since the unique element distribution pattern for the contaminant background is not limited to Stardust allocation C2092,2,80,47,6 there is the likelihood of a common Stardust background.

Acknowledgments—I am grateful for the comments and suggestion of George Flynn, Mike Zolensky, and handling editor. This work was supported by NASA grant NNX07AM65G through the NASA Stardust Analyses Program. The analyses were conducted in the Electron Microbeam Analyses Facility in the Department of Earth and Planetary Sciences at UNM.

Editorial Handling—Dr. Scott Sandford

REFERENCES

Anders E. and Grevesse N. 1989. Abundances of the elements: Meteoritic and solar. *Geochimica et Cosmochimica Acta* 53: 197–214.

Bradley J. P. 1988. Analysis of chondritic interplanetary dust thin-sections. *Geochimica et Cosmochimica Acta* 52:889–900.

Bradley J. P. 1994. Chemically anomalous, pre-accretionally irradiated grains in interplanetary dust from comets. *Science* 265: 925–929.

Bradley J. P. and Ishii H. A. 2008. Comment on "The shape and composition of interstellar silicate grains." *Astronomy & Astrophysics* 486:781–784.

Brownlee D., Tsou P., Aléon J., Alexander C. M. O' D., Araki T., Bajt S., Baratta G. A., Bastien R., Bland Ph., Bleuet P., Borg J., Bradley J. P., Brearley A., Brenker F., Brennan S., Bridges J. C., Browning N. D., Brucato J. R., Bullock E., Burchell M. J., Busemann H., Butterworth A., Chaussidon M., Cheuvront A., Chi M., Cintala M. J., Clark B. C., Clemett S. J., Cody G., Colangeli L., Cooper G., Cordier P., Daghlian C., Dai Z., D'Hendecourt L., Djouadi Z., Dominguez G., Duxbury T., Dworkin J. P., Ebel D. S., Economou T. E., Fakra S., Fairey S. A. J., Fallon S., Ferrini G., Ferroir T., Fleckenstein H., Floss C., Flynn G., Franchi I. A., Fries M., Gainsforth Z., Gallien J.-P., Genge M., Gilles M. K., Gillet P., Gilmour J., Glavin D. P., Gounelle M., Grady M. M., Graham G. A., Grant P. G., Green S. F., Grossemy F., Grossman L., Grossman J. N., Guan Y., Hagiya H., Harvey R., Heck P., Herzog G. F., Hoppe P., Hörz F., Huth J., Hutcheon I. D., Ignatyev K., Ishii H., Ito M., Jacob D., Jacobsen C., Jacobsen S., Jones S., Joswiak D., Jurewicz A., Kearsley A. T., Keller L. P., Khodja H., Kilcoyne A. L. D., Kissel J., Krot A., Langenhorst F., Lanzirotti A., Le L., Leshin L. A., Leitner J., Lemelle L., Leroux H., Liu M-C., Luening K., Lyon I., MacPherson G., Marcus M. A., Marhas K., Marty B., Matrajt G., McKeegan K., Meibom A., Mennella V., Messenger K., Messenger S., Mikouchi T., Mostefaoui S., Nakamura T., Nakano T., Newville M., Nittler L. R., Ohnishi I., Ohsumi K., Okudaira K., Papanastassiou D. A., Palma R., Palumbo M. E., Pepin R. O, Perkins D., Perronnet M., Pianetta P., Rao W., Rietmeijer F. J. M., Robert F., Rost D., Rotundi A., Ryan R., Sandford S. A., Schwandt G. S., See T. H., Schlutter D., Sheffield-Parker J., Simionovici A., Simon S., Sitnitsky I., Snead C. J., Spencer M. K., Stadermann F., Steele A., Stephan T., Stroud R., Susini J., Sutton S. R., Suzuki Y., Taheri M., Taylor S., Teslich N., Tomeoka K., Tomioka N., Toppani A., Trigo-Rodríguez J. M., Troadec D., Tsuchiyama A., Tuzzolino A. J., Tyliszczak T., Uesugi K., Velbel M., Vellenga J., Vicenzi E., Vincze L., Warren J., Weber I., Weisberg M., Westphal A. J., Wirick S., Wooden D., Wopenka B., Wozniakiewicz P., Wright I., Yabuta H., Yano H., Young E. D., Zare R. N., Zega T., Ziegler K., Zimmerman L., Zinner E., and Zolensky M. 2006. Comet 81P/Wild 2 under a microscope. *Science* 314:1711–1716.

Flynn G. J., Bleuet P., Borg J., Bradley J. P., Brenker F. E., Brennan S., Bridges J., Brownlee D. E., Bullock E. S., Burghamme M., Clark B.C., Dai Z. R., Daghlian C. P., Djouadi Z., Fakra S., Ferroir T., Floss C., Franchi I. A., Gainsforth Z., Gallien J. P., Gillet Ph., Grant P. G., Graham G. A., Green S. F., Grossemy F., Heck P. R., Herzog G. F., Hoppe P., Hörz F., Huth J., Ignatyev K., Ishii H. A., Janssens K., Joswiak D., Kearsley A. T., Khodja H., Lanzirotti A., Leitner J., Lemelle L., Leroux H., Luening K., MacPherson G. J., Marhas K. K., Marcus M. A., Matrajt G., Nakamura T., Nakamura-Messenger K., Nakano T., Newville M., Papanastassiou D. A., Pianetta P., Rao W., Riekel C., Rietmeijer F. J. M. , Rost D., Schwandt G. S., See T. H., Sheffield-Parker J., Simionovici A., Sitnitsky I., Snead C. J., Stadermann F. J., Stephan T., Stroud R. M., Susini J., Suzuki Y., Sutton S. R., Taylor S., Teslich N., Troadec D., Tsou P., Tsuchiyama A, Uesugi K., Vekemans B., Vicenzi E. P., Vincze L., Westphal A. J., Wozniakiewicz P., Zinner E., and Zolensky M. E. 2006. Elemental compositions of comet 81P/Wild 2 samples collected by Stardust. *Science* 314:1731–1735.

Ishii H. A., Brennan S., Bradley J. P., Luening K., Ignatyev K., and Pianetta P. 2008a. Recovering the elemental composition of comet Wild 2 dust in five Stardust impact tracks and terminal particles in aerogel. *Meteoritics & Planetary Science* 43:215–231.

Ishii H. A., Bradley J. P., Dai Z. R., Chi M., Kearsley A. T., Burchell M. J., Browning N. D., and Molster F. 2008b. Comparison of comet 81P/Wild 2 dust with interplanetary dust from comets. *Science* 319:447–450.

Joswiak D. J., Brownlee D. E., Bradley J. P., Schlutter D. J., and Pepin R. O. 1996. Systematic analyses of major element distributions in GEMS from high speed IDPs (abstract). 27th Lunar and Planetary Science Conference. pp. 625–626.

Lanzirotti A., Sutton S. R., Flynn G. J., Newville M., and Rao W. 2008. Chemical composition and heterogeneity of Wild 2 cometary

particles determined by synchrotron X-ray fluorescence. *Meteoritics & Planetary Science* 43:197–213.

Leroux H., Rietmeijer F. J. M., Velbel M. A., Brearley A. J., Jacob D., Langenhorst F., Bridges J. C., Zega T. J., Stroud R. M., Cordier P., Harvey R. P., Lee M., Gounelle M., and Zolensky M. E. 2008. A TEM study of thermally modified comet 81P/Wild 2 dust particles by interactions with the aerogel matrix during the Stardust capture process. *Meteoritics & Planetary Science* 43: 97–120.

Matrajt G., Ito M., Wirick S., Messenger S., Brownlee D. E., Joswiak D., Flynn G., Sandford S., Snead C., and Westphal A. 2008. Carbon investigation of two Stardust particles: A TEM, NanoSIMS, and XANES study. *Meteoritics & Planetary Science* 43:315–334.

Nakamura T., Tsuchiyama A., Akaki T., Uesugi K., Nakano T., Takeuchi A., Suzuki Y., and Noguchi T. 2008. Bulk mineralogy and three-dimensional structures of individual Stardust particles deduced from synchrotron X-ray diffraction and microtomography analysis. *Meteoritics & Planetary Science* 43: 247–259.

Rietmeijer F. J. M. 1989. Ultrafine-grained mineralogy and matrix chemistry of olivine-rich chondritic interplanetary dust particles. Proceedings, 19th Lunar and Planetary Science Conference, edited by Ryder G. and Sharpton V. L. Cambridge University Press and The Lunar and Planetary Institute. pp. 513–521.

Rietmeijer F. J. M. 1993. Size distributions in two porous chondritic micrometeorites. *Earth and Planetary Science Letters* 117: 609–617.

Rietmeijer F. J. M. 1994. Searching for a principal component mixing model for chondritic interplanetary dust particles: The use of size analysis (abstract). 25th Lunar and Planetary Science Conference. pp. 1129–1130.

Rietmeijer F. J. M. 1996a. Cellular precipitates of iron-oxide in olivine in a stratospheric interplanetary dust particle. *The Mineralogical Magazine* 60:877–885.

Rietmeijer F. J. M. 1996b. The butterflies of principal components: A case of ultrafine-grained polyphase units (abstract). 27th Lunar and Planetary Science Conference. pp. 1073–1074.

Rietmeijer F. J. M. 1998. Interplanetary dust particles. In *Planetary materials*, edited by J. J. Papike. Chantilly, Virginia: Mineralogical Society of America. Reviews in Mineralogy, vol. 36. pp. 2-1–2-95.

Rietmeijer F. J. M. 1999. Metastable non-stoichiometric diopside and Mg-wollastonite: An occurrence in an interplanetary dust particle. *American Mineralogist* 84:1883–1894.

Rietmeijer F. J. M. 2002. The earliest chemical dust evolution in the solar nebula. *Chemie der Erde* 62:1–45.

Rietmeijer F. J. M. 2004. Dynamic pyrometamorphism during atmospheric entry of large (~10 micron) pyrrhotite fragments from cluster IDPs. *Meteoritics & Planetary Science* 39:1869–1887.

Rietmeijer F. J. M. 2007. Challenges to understand aerogel contaminated by hypervelocity-impacted comet Wild 2 dust (abstract #1082). 38th Lunar and Planetary Science Conference. CD-ROM.

Rietmeijer F. J. M. 2008. Time, temperatures, and pressure indicated by metastable iron-sulfide nanophases in melted Stardust aerogel (abstract #1188). 39th Lunar and Planetary Science Conference. CD-ROM.

Rietmeijer F. J. M. 2009. A cometary aggregate interplanetary dust particle as an analog for comet Wild 2 grain chemistry preserved in silica-rich Stardust glass. *Meteoritics & Planetary Science* 44.

Rietmeijer F. J. M. and Nuth III J. A. 2004. Grain sizes of ejected comet dust: Condensed dust analogs, interplanetary dust particles and meteors. In *The new ROSETTA targets—Observation, simulations and instrument performances*, edited by Colangeli L., Mazzotta Epifani E., and Palumbo P. Astrophysics and Space Science Library, Kluwer Academic Publishers. pp. 97–110.

Rietmeijer F. J. M., Nuth III J. A., Karner J. M., and Hallenbeck S. L. 2002. Gas to solid condensation in a Mg-SiO-H_2-O_2 vapor: Metastable eutectics in the MgO–SiO_2 phase diagram. *Physical Chemistry Chemical Physics* 4:546–551.

Rietmeijer F. J. M., Nakamura T., Tsuchiyama A., Uesugi K., Nakano T., and Leroux H. 2008. Origin and formation of iron-silicide phases in the aerogel of the Stardust mission. *Meteoritics & Planetary Science* 43:121–134.

Stephan T., Rost D., Vicenzi E. P., Bullock E. S., MacPherson G. J., Westphal A. J., Snead C. J., Flynn G. J., Sandford S. A., and Zolensky M. E. 2008. TOF-SIMS analysis of cometary matter in Stardust aerogel tracks. *Meteoritics & Planetary Science* 43: 233–246.

Tomeoka K., Tomioka N., and Ohnishi I. 2008. Silicate minerals and Si-O glass in comet Wild 2 samples: Transmission electron microscopy. *Meteoritics & Planetary Science* 43:273–284.

Tsou P., Brownlee D. E., Hörz F., Sandford S. A., and Zolensky M. E. 2003. Wild 2 and interstellar sample collection and Earth return. *Journal of Geophysical Research* 108:E8113.

Zolensky M. and Barrett R. 1994. Compositional variations of olivines and pyroxenes in chondritic interplanetary dust particles. *Meteoritics* 29:616–620.

Zolensky M. E., Zega T. J., Yano H., Wirick S., Westphal A. J., Weisberg M. K., Weber I., Warren J. L., Velbel M. A., Tsuchiyama A., Tsou P., Toppani A., Tomioka N., Tomeoka K., Teslich N., Taheri M., Susini J., Stroud R., Stephan T., Stadermann F. J., Snead C. J., Simon S. B., Simionovici A., See T. J., Robert R., Rietmeijer F. J. M., Rao W., Perronnet M. C., Papanastassiou D. A., Okudaira K., Ohsumi K., Ohnishi I., Nakamura-Messenger K., Nakamura T., Mostefaoui S., Takashi Mikouchi T., Meibom A., Matrajt G., Marcus M. A., Leroux H., Lemelle L., Le L., Lanzirotti A., Langenhorst F., Krot A. N., Keller L. P., Kearsley A. T., Joswiak D., Jacob D., Ishii H., Harvey R., Hagiya K., Grossman L., Grossman J. N., Graham G. A., Gounelle M., Gillet P., Genge M. J., Flynn G., Ferroir T., Fallon S., Ebel D. S., Dai Z., Cordier P., Clark B., Chi1 M., Butterworth A. L., Brownlee D. E., Bridges J. C., Brennan S., Brearley A., Bradley J. P., Bleuet P., Bland P. A., and Bastien R. 2006. Mineralogy and petrology of comet Wild 2 nucleus samples. *Science* 314:1735–1739.

Zolensky M., Nakamura-Messenger K., Sverdrup J., Rietmeijer F., Leroux H., Mikouchi T., Ohsumi K., Simon S., Grossman L., Stephan T., Weisberg M., Velbel M., Zega T., Stroud R., Tomeoka K., Ohnishi I., Tomioka N., Nakamura T., Matrajt G., Joswiak J., Brownlee D., Langenhorst F., Krot A., Kearsley A., Ishii H., Graham G., Dai Z. R., Chi M., Bradley J., Hagiya K., Gounelle M., and Bridges J. 2008. Comparing Wild 2 particles to chondrites and IDPs. *Meteoritics & Planetary Science* 43:261–272.